Creation of a high-temperature plasma through merging and compression of supersonic field reversed configuration plasmoids

2011 Nucl. Fusion 51 053008

(http://iopscience.iop.org/0029-5515/51/5/053008)

IOP Publishing and International Atomic Energy Agency Nuclear Fusion
Nucl. Fusion **51** (2011) 053008 (10pp) doi:10.1088/0029-5515/51/5/053008

Creation of a high-temperature plasma through merging and compression of supersonic field reversed configuration plasmoids

John Slough, George Votroubek and Chris Pihl

MSNW LLC, 8551 154th Avenue NE, Redmond, WA 98052, USA

E-mail: sloughj@msnwllc.com

Received 30 November 2010, accepted for publication 8 March 2011
Published 13 April 2011
Online at stacks.iop.org/NF/51/053008

Abstract
A new device, the Inductive Plasma Accelerator, was employed to simultaneously form and accelerate two oppositely directed field reversed configurations (FRCs) where the relative velocity (600 km s^{-1}) of the plasmoids was much larger than their internal thermal motion. Upon collision all of the FRC directional energy was observed to be rapidly thermalized concurrent with complete magnetic reconnection of the two FRCs. Upon merging, the resulting FRC was compressed to kilovolt ion temperatures exhibiting a configuration lifetime better than predicted by past scaling of *in situ* formed FRCs. With the improved FRC confinement scaling, a pulsed plasma device based on this approach capable of achieving fusion gain is examined. For an FRC with a poloidal flux 20 mWb or greater, the fusion energy yield per pulse exceeds the plasma energy for compression fields of 10 T or more. The scaling is insensitive to the compression chamber radial scale, providing for the possibility of a very compact fusion neutron source.

(Some figures in this article are in colour only in the electronic version)

1. Introduction

The field reversed configuration (FRC) is a plasmoid with a symmetric toroidal geometry in which the confining magnetic field is provided by toroidal plasma currents [1]. The plasma pressure is contained by the encompassing magnetic pressure and magnetic tension with the result that the plasma energy is comparable to the FRC field energy (the ratio is commonly referred to as the plasma β and is $\sim$1 for the FRC). An illustration of the FRC along with the key equations describing the FRC equilibrium can be found in figure 1. These features make the FRC the geometrically simplest, most compact, and highest β of all magnetic confinement schemes. The simply connected nature of the magnetic field with regard to the containment vessel and the linear confinement geometry, allow for the translation of the FRC over large distances. These attributes make the FRC especially attractive as a means to contain thermonuclear plasmas. These unique qualities, however, are obtained at a price. The topological simplicity makes the generation and sustainment of the large diamagnetic currents very challenging. The configuration has net bad magnetic curvature and is susceptible to magnetohydrodynamic (MHD) interchange and kink modes. When isolated from the vessel wall by an external axial magnetic field, as is typically the case, the FRC poloidal field represents essentially an anti-aligned dipole with regard to the external field and is therefore disposed to tilt instability.

Despite these daunting issues, stable high-temperature FRC plasmoids have been readily formed where the requisite plasma heating and current generation was produced by rapid reversal of the axial magnetic field in cylindrical coil geometry. Once formed, the FRC is observed to be stable and the plasma well confined as long as the plasma remains in a kinetic regime. This regime is characterized by S^*, the ratio of the FRC separatrix radius r_s and the ion collisionless skin depth c/ω_{pi}. Past FRC scaling has shown that stable FRCs can be formed at low flux where ion kinetic effects dominate. Both stability and transport are observed to rapidly deteriorate when the kinetic condition $S^*/\varepsilon > 5$ was exceeded. Here ε is the FRC separatrix elongation ε $(=l_s/2r_s)$ [2]. In any case the FRC decays on a resistive time scale that is anomalous. FRC confinement in the kinetic regime was initially observed to scale roughly as $\tau \sim r^2/\rho_i$ [3] where ρ_i is the ion Larmour radius at the FRC separatrix. Since the FRC has primarily only a poloidal magnetic field, the plasma pressure at the null must equal the radial pressure exerted by the external field in

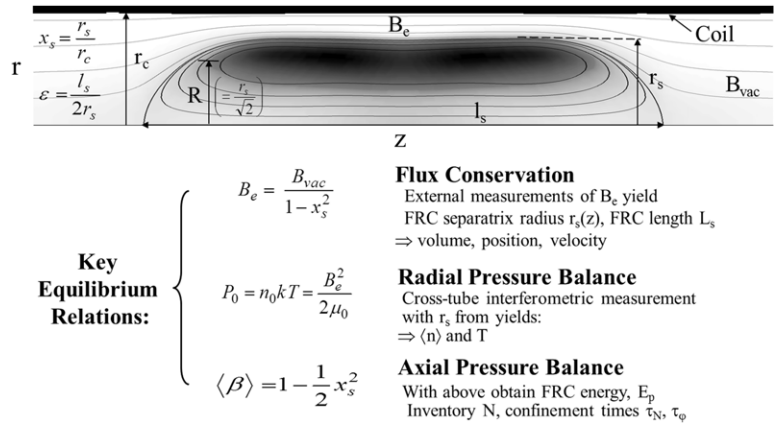

Figure 1. Top: field lines and pressure contours for the FRC with the characteristic scaling parameters indicated. Bottom: FRC equilibrium constraints and the diagnostic measurements that together with the equilibrium relations that are employed to determine the basic parameters of the FRC equilibrium.

equilibrium,

$$B_e^2 = 2\mu_0 n_0 k(T_e + T_i), \quad (1)$$

where the zero subscript refers to the value at the magnetic null radius R ($=r_s/\sqrt{2}$). With $T_i \sim T_e$ one has $1/\rho_i \sim n^{1/2}$ inferring that the diffusion coefficient for the FRC is independent of radial scale and has only a positive scaling with density. Later results on LSX [4] and other experiments indicated further dependences with the FRC elongation, ε and the ratio of FRC separatrix radius r_s to coil radius r_c, with this ratio designated as x_s.

The observed particle confinement, stated in terms of directly measured quantities, that can be accurately measured across all experiments, yields the following scaling [5]:

$$\tau_N = 3.2 \times 10^{-15} \varepsilon^{0.5} x_s^{0.8} r_s^{2.1} n^{0.6}, \quad (2)$$

where x_s is the ratio of the FRC separatrix radius, r_s, to coil radius, r_c. With reasonable assumptions for the FRC relative size and shape ($\varepsilon \sim 15$ and $x_s = 0.6$), this scaling, together with kinetic condition, determines the plasma radius and density required to satisfy the Lawson criteria for fusion gain, i.e. $n_0 \geqslant 1.5 \times 10^{23}\,\mathrm{m}^{-3}$ and $r_s \leqslant 7.0\,\mathrm{cm}$. The high plasma energy density implied by these constraints prescribes a small, pulsed fusion regime for the FRC. These FRC parameters, together with the required temperature and confinement, however, have not been obtained by any of the formation methodologies that have been employed in past experiments.

2. Experiment

The ability of the FRC plasmoid to be translated several metres allows for the FRC formation and kinetic energy for heating to be realized outside of the burn chamber and breeding blanket. The high energy density state can then be obtained through the rapid conversion of the FRC axial kinetic energy. The experiments to be described here were instigated to examine the physics of this process. To accomplish this, a new device was constructed and is referred to as the Inductive Plasma Accelerator (IPA) [6]. The initial configuration was equipped with an enlarged merging chamber as illustrated in figure 2.

To minimize the formation time, as well as maximize the FRC acceleration, the IPA device was constructed so that a new formation methodology could be employed, which is referred to as dynamic formation [7]. The monolithic theta pinch coil, utilized for FRC formation in virtually all previous FRC experiments [1], was replaced by a set of electrically isolated and independently triggered formation/acceleration coils. In the initial setup five such coils were employed, and all were supplied with an initial reverse bias field ~0.06 T. A forward bias was applied to the end coils as well as the coils in the merging/compression section. For the compression experiments, the formation section was increased in radius to provide for greater initial FRC flux and energy. This was followed at smaller radius by a set of pure accelerator coils with positive bias for the addition of kinetic energy after FRC formation. The merging/compression chamber was reduced to this smaller radius as well (see figure 3). For both configurations the formation coils were energized sequentially to both form and accelerate the FRC simultaneously. By executing field reversal in this sequenced fashion the FRC flux can be maintained throughout the entire process [7]. The terminal FRC velocity was $210\,\mathrm{km\,s^{-1}}$ with the initial configuration and as high as $300\,\mathrm{km\,s^{-1}}$ in the final configuration with additional accelerator coils.

The initial plasma was generated by an annular array of 16 small coaxial plasma guns located near the quartz vacuum tube wall under the first formation coil (see figure 3). These devices were each inductively isolated and pulsed at high current (3–6 kA) and produced a fully ionized plasma flowing at roughly $2\,\mathrm{cm}\,\mu\mathrm{s}^{-1}$. The plasma guns were based on the magnetoplasmadynamic (MPD) thruster [8] which produces a fully ionized plasma, and the absence of significant neutral flow prior to initiation was characterized in separate experiments. The ejected plasma coalesced to form an annular plasma as indicated by end-on framing pictures. This provided for good flux trapping on reversal as indicated by the large excluded flux signal during reversal, and the formation of a more oblate FRC for acceleration. The use of plasma guns in this manner also provided for a means to keep the merging chamber and accelerator at high vacuum. This was important as a significant neutral density considerably affected FRC behaviour that prevented both FRC merging and the

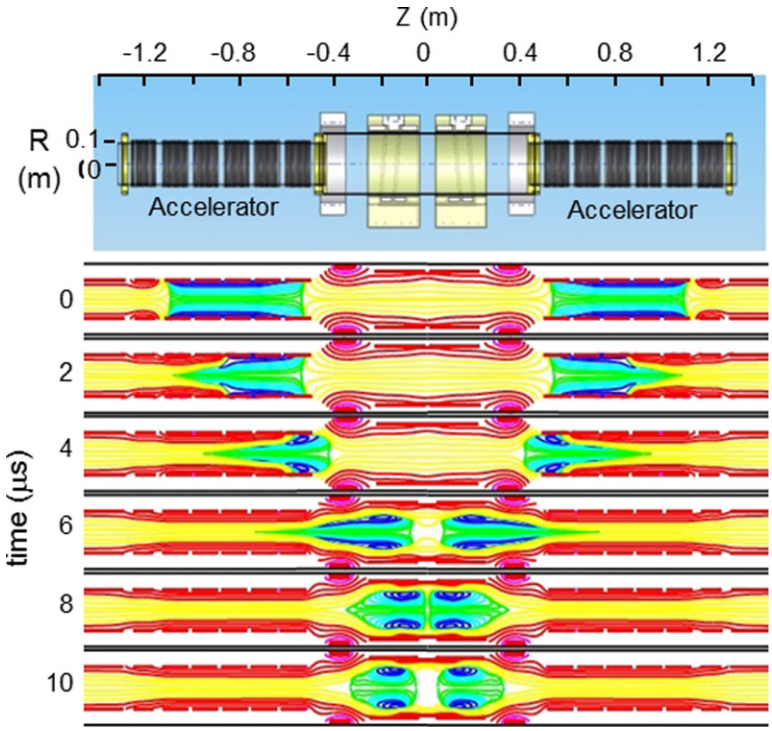

Figure 2. Initial configuration of the IPA device and flux contours from numerical calculations based on experimental conditions for FRC dynamic formation and merging.

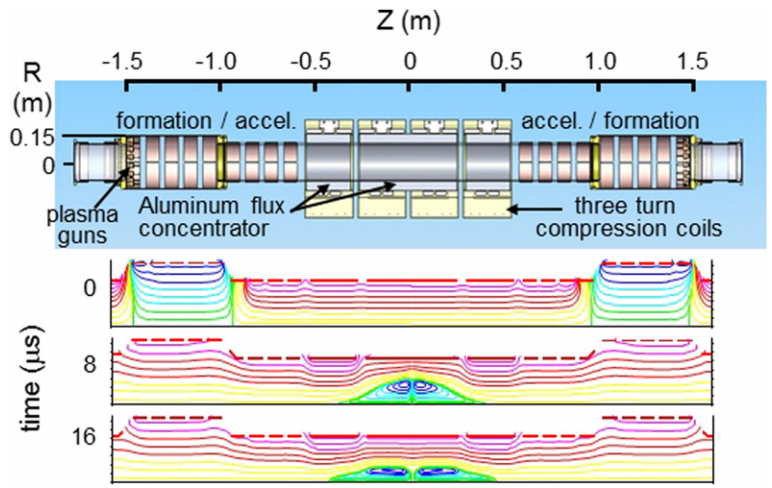

Figure 3. IPA configuration for FRC acceleration, merging and compression. The flux contours from the MHD calculations correspond to the initial magnetic field structure (0), the peak axial compression (8) and magnetic compression (16).

establishment of an equilibrium of any significant duration as indicated by the diamagnetic signals in the compression section.

In the initial experimental configuration, the FRC was dynamically formed and injected into a larger chamber to study the merging process without the complications of compression and additional acceleration. The merging chamber consisted of a 0.14 m radius quartz cylinder lined with a 0.3 m long cylindrical, thin tungsten liner. A suitable bias field of 0.1–0.2 T was embedded inside this liner to radially confine the FRC plasmas during merging, while two multi-turn coils provided for a small mirror field (∼0.2 T) on either end of the chamber. An array of external flux and B_z field loops were installed under each coil as well as an axial array of B_z probes inside the tungsten shell. From this array the excluded flux due to the presence of the FRC was obtained, and the FRC velocity, radius, length and energy were determined. A HeNe laser-based interferometer measured the cross tube line density at the axial midplane. From this diagnostic and the magnetic measurements, the plasma density and pressure balance temperature were obtained. Deuterium plasmas were employed and a calibrated neutron detector was positioned radially outside the magnets at the chamber centre to measure the D–D fusion neutron flux.

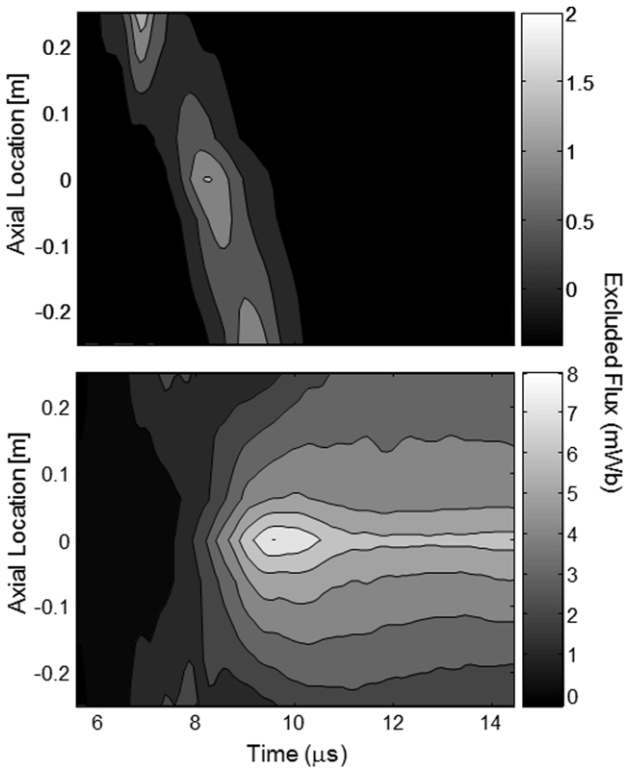

Figure 4. Excluded flux from diagnostic array in merging chamber for the experimental configuration shown in figure 1 for (top) single FRC passage, and (bottom) colliding FRCs.

The ratio of FRC directed velocity to thermal velocity was found to be greater than three. The merging and conversion of the FRC kinetic energy was observed to take place on the Alfvénic timescale. The distinct difference between merging and the simple passage of the FRC unopposed is clearly demonstrated in the array of excluded flux signals in the interaction chamber as illustrated in figure 4. The two FRCs merged as they collided to form a single FRC indicated by the peak diamagnetism appearing and remaining at the axial midplane. It is worth noting that with merging the excluded flux increased by a factor of at least four greater than observed for the transiting FRC.

In a constant flux cylindrical coil the thermal conversion of kinetic energy would be manifested by a large increase in plasma length as the equilibrium axial magnetic pressure constraint determines the FRC average beta [3],

$$\langle\beta\rangle = 1 - \frac{1}{2}x_s^2. \tag{3}$$

An increase in plasma radius indicated by the significantly increased excluded flux signal would normally only occur from a large increase in poloidal flux. This large increase in excluded flux has also been observed in some translation experiments where a single FRC expands and comes to rest to fill a large chamber, and has been attributed to the possible conversion of toroidal flux into poloidal flux [9, 10]. Based on the results here, however, this is not likely to be the correct explanation for several reasons. Any formation-induced toroidal flux is oppositely directed for each of the merging FRCs and would be annihilated with merging as observed in spheromak counter helicity merging [11].

There is a more plausible explanation for the increased plasma radius than an increase in flux. If the equilibrium length of the FRC were to expand beyond the region over which the flux is held constant, the changing end conditions will significantly affect the average beta. In equilibrium the plasma pressure along a field line is constant, and must also be in radial pressure balance with the local external field, or $B_{\rm end} = B_{\rm e} = B_{\rm vac}/(1 - x_s^2)$. At this critical value an average beta condition can be derived from the Maxwell stress tensor in a manner similar to that obtained for constant axial flux [3] with the result:

$$\langle\beta\rangle_0 = 1 - \tfrac{1}{2}x_{s0}^2 R^4, \tag{4}$$

where R is the ratio of the FRC separatrix in the end region to that at the midplane. If the region at the end of the FRC is maintained with a magnetic field that is greater than the external field at the FRC midplane ($B_{\rm end} > B_{\rm e}$) the FRC is forced to contract axially and expand radially. With a large increase in plasma energy from thermal conversion, the FRC must expand in radius compressing the axial field between the FRC and flux conserving coil until $B_{\rm e} \sim B_{\rm end}$. At this point the FRC can expand axially and equation (4) will hold. In this case, the FRC is characterized by a higher β than given by the constant axial flux relation in equation (3).

The interpretation of the IPA experimental results was considerably aided by the use of 2D resistive MHD calculations performed with the Moqui code [12]. By initializing the code with the experimental magnetic waveforms from the experiments, the dynamic behaviour of the FRC formation, acceleration and velocity was matched by adjusting the initial flux and plasma inventory. The same large increase in excluded flux is observed in the code on thermalization as it was in the experiments with no change in the total poloidal flux, thus confirming the interpretation given here.

There was one significant difference between the code and the observed behaviour of the colliding FRCs as can be seen in the results of the calculations shown in figure 2. Complete merging was not produced in the code whereas it was always observed in the experiments. In the code the FRC kinetic energy is almost completely thermalized upon collision (>99%), but the small residual rebound velocity of several km s^{-1} causes immediate separation of the FRCs prohibiting further reconnection, and undoing whatever reconnection that had occurred. Magnetic reconnection is one of the central processes in plasma physics. One of the key issues in understanding magnetic reconnection is what determines the magnitude of the reconnection rate. In simple two-dimensional models as employed here, the reconnection site is characterized by a local null point of the magnetic field with field lines extending from the null forming an x-type separatrix. In resistive MHD models of reconnection this rate is controlled by the magnitude of the resistivity. However, modifying the resistivity in the Moqui code, even with density weighted resistivities, it was not possible to obtain complete reconnection of the merging FRCs. This is counter to the resistively driven reconnection model found to explain the reconnection rates observed in merging spheromak experiments [13]. The observed rate in spheromak reconnection is far too slow to explain the rate observed in the experiments here where the FRC is found to reconnect at Alfvénic ($M_{\rm A} \sim 1$) speed.

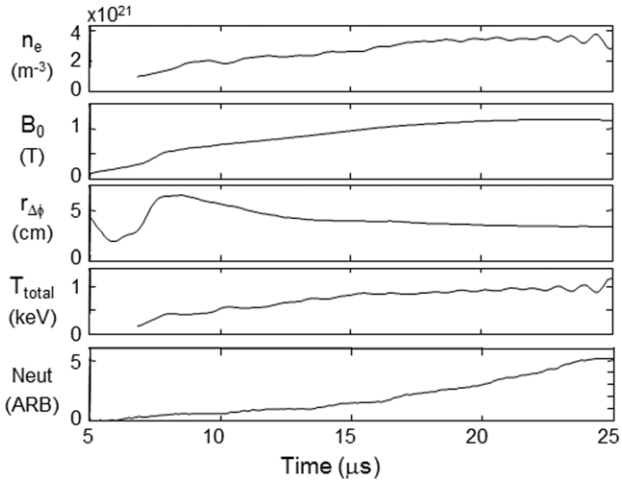

Figure 5. FRC experimental data at the axial midplane during compression for the IPA configuration shown in figure 2. Plotted from top to bottom: the radially averaged electron density, the axial magnetic field external to the FRC, the excluded flux (plasma) radius, the radially averaged total plasma temperature, and the D–D fusion neutron signal detected by a scintillator-based neutron detector.

In contrast to typical resistive models, numerical simulations of collisionless reconnection have demonstrated that magnetic reconnection in sufficiently thin current sheets, in which Hall effects and whistler dynamics become important, may occur at a fast rate that does not depend on the dissipation mechanism. The reconnection rates predicted from codes with the Hall term, as well as pure particle codes, predict reconnection on timescales of 30–50 ω_{ci}^{-1} [14]. The ion cyclotron time, ω_{ci}^{-1}, at peak axial compression was 1 and 0.1 μs for the expansion merging and compression merging experiments, respectively. Again, the reconnection timescale predicted is very long. The likely explanation is that the reconnection is inherently three dimensional, and that the local resistivity may be highly anomalous. Work is currently underway at the University of Washington employing a 3D MHD code referred to as NIMROD [15, 16] which includes both the Hall and resistive terms. Hopefully this code can shed more light on the exact mechanism at play here.

The basic FRC equilibrium parameters observed during compression are displayed in figure 5.

Total temperature was calculated based on radial pressure balance. During compression it can be seen that this resulted in total temperatures of 1 keV or more. The overwhelmingly larger ion mass dictates that the ions receive virtually all the heating from kinetic conversion of the FRC motion. The MHD calculations reflect this with ion temperatures $T_i \sim 850$ eV after collision and compression. A strong neutron signal was detected during magnetic compression from two calibrated scintillator-based detectors, manufactured by Eljen Technology. These detectors were employed at the axial midplane to monitor the time history of the neutron flux. The EJ-410 detector employed is specifically designed for detecting fast neutrons while being nearly insensitive to gamma radiation. The detector consists of zinc sulfide phosphor embedded in a hydrogenous polymer matrix structured in a series of concentric cylinders of clear plastic to facilitate light collection. The fast neutron detector is directly mounted to a photomultiplier with a time response of 0.2 μs (scintillator decay constant). A Monte Carlo N Particle (MCNP) transport code was employed to correct for neutron passage through the quartz tube, aluminium magnets as well as the lead shielding placed around the neutron detector itself. Scattering and slowing from surrounding structures accounted for about a factor of two reduction in neutrons detected on IPA according to the MCNP calculations. Even with correction for FRC geometry, attenuation and scattering in intervening material a much higher ion temperature, $T_i \sim 2$ keV, was inferred. The anomalously large signal was well beyond what could be attributed to measurement error of the plasma density and volume. Most likely it is the result of a non-thermal ion population, but the mechanism for maintaining this over the ~30 μs of the FRC compression time is not clear.

The confinement observed for the merged and compressed FRC was better than the scaling inferred from equation (2) by roughly a factor of 2 for the conditions shown in figure 5. This scaling was based on FRCs confined in constant flux coils. Enhanced confinement has also been observed in translation experiments where the FRC is expanded into, and completely fills a larger chamber [9, 10]. It would be tempting to attribute the improved confinement to flux generation, but as discussed, this interpretation is not warranted when the FRC is mirror confined. Previous compression experiments of a translated FRC into a constant flux coil did not exhibit enhanced confinement [17]. Mirror confinement provides several possible mechanisms that could lead to improved confinement. It produces a stronger magnetic nozzle at the ends of the FRC slowing the open field line plasma loss, which in turn relaxes the large radial pressure gradient across the separatrix that would suppress instabilities such as lower hybrid drift that has been calculated to produce the transport scaling observed for FRCs. The increased plasma radius and beta reduce the magnetic gradient at the null and could thus reduce the flux loss for the same plasma resistivity.

The rotational instability that is always observed later in the equilibrium with FRCs formed *in situ* was observed in the merged FRC experiments with compression, but not expansion. The rotational instability occurs when α, the ratio of the plasma rotation compared with the ion diamagnetic drift frequency, approaches one. For the rigid rotor profile it can be shown that $\alpha \propto L/x_s^2$ [3]. The experimental results are in accord with this scaling if it is assumed that the angular momentum L acquired by the FRC is similar for both cases. It has been shown that a significant toroidal field can stabilize this mode [18], so that the observed spin up under compression would indicate that little toroidal field is present after merging.

3. FRC fusion scaling

The fusion reaction rate, dN_{fus}/dt (n s^{-1}), for D–T fusion systems is given by

$$\frac{dN_{fus}}{dt} = \int_{vol} n_D n_T \langle \sigma v \rangle \, dVol, \tag{5}$$

where n_α is the number density of species α, and $\langle \sigma v \rangle$ is the reaction rate parameter for the fusion reaction of interest for

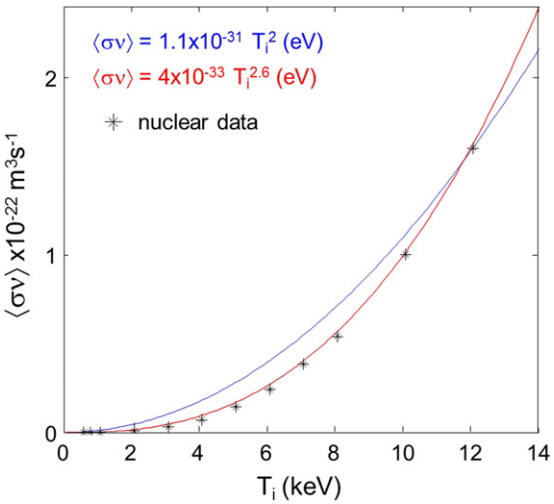

Figure 6. Nuclear cross section for D–T fusion and approximate fits over range of interest for pulsed FRC fusion.

a plasma with ion temperature T_i. It will be assumed that $n_D = n_T = 1/2\,n$ where n is the total ion density. For pulsed systems such as the IPA-based FRC device considered here, the relevant quantity is the total neutron yield per pulse. Equation (5) should thus be integrated over the lifetime of the plasmoid and then multiplied by the repetition rate R_p to obtain the neutron flux. For the purposes here it will be sufficient to multiply the left-hand side of equation (5) by the energy confinement time. The energy confinement is typically 2/3 of the particle confinement time [19], and the particle confinement for merged FRCs was found to be roughly a factor of two better than the expression in equation (2). During the decay of the FRC the plasma density and temperature are maintained as the product must be in radial pressure balance with the external magnetic field (see figure 1). The total fusion energy provided by the D–T reaction is $E_{fus} = N_{fus}\cdot(22.4\,\mathrm{MeV})\cdot(1.6\times10^{-13}\,\mathrm{J\,MeV^{-1}})$. This includes an additional 4.8 MeV from the lithium fusion in the blanket required to obtain a new triton for continued operation of the reactor. With this one can write for the FRC:

$$P_{fus} \cong 1.2\times10^{-12} n^2 \langle\sigma v\rangle \tau_N \mathrm{Vol}_{FRC} R_p. \qquad (6)$$

For the highly elongated FRC, the volume can be approximated $\mathrm{Vol}_{FRC} = \pi r_s^2 l_s$. For temperatures between 10 and 20 keV, the usual approximation for the D–T fusion cross section is $\langle\sigma v\rangle \cong 1.1\times10^{-31} T_i^2$ (eV). It is clearly desirable to operate at the upper limit in magnetic field pressure as this maximizes the fusion yield. Since increasing the ion temperature comes at the expense of decreasing n for a given magnetic pressure (see equation (1)) there is thus no advantage in seeking higher ion temperatures. In fact there is a disincentive in that the FRC lifetime also decreases with decreasing n. It turns out that for ion temperatures in the range 3–12 keV, the range anticipated for the optimal operation of the IPA device, a fit to the cross section is better approximated by $\langle\sigma n\rangle \cong 4\times10^{-33} T_i^{2.6}$ (eV) as is indicated in figure 6.

Given the FRC confinement scaling, and the ion temperature within this range, the neutron yield is essentially independent of the ion temperature. More precisely, the increase in fusion cross section at higher temperature is offset by decreased density and FRC lifetime at a given compression magnetic field.

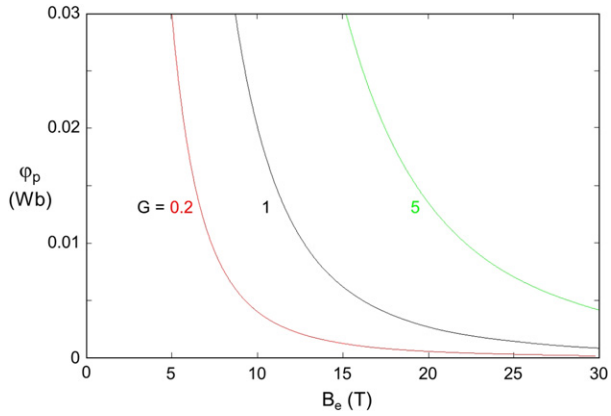

Figure 7. Gain contours as a function of the FRC poloidal flux and compression magnetic field. It was assumed that the FRC length $l_s = 1$ m.

While the physical dependences for all terms in equation (6) have been identified, it is worth introducing quantities that are primarily determined by the device parameters that can be changed and optimized. The fundamental parameters in this regard are the compression magnetic field, B_e, the compression coil radius, r_c, and the magnitude of the FRC poloidal flux, φ_p. Assuming that the current profile is similar to the rigid rotor profile commonly inferred by observed pressure profiles [20], the closed poloidal flux, along with B_e and r_c, in turn determines the plasma radius, r_s, as

$$\varphi_p \cong \frac{r_s^3}{r_c} B_e \Rightarrow r_s = \left(\frac{r_c \varphi_p}{B_e}\right)^{1/3}. \qquad (7)$$

With equation (7) for the FRC radius, and solving equation (1) for the density, along with the appropriate approximation for the D–T cross section as stated above, the FRC fusion energy per pulse (from equation (6)) can be rewritten in terms of the experimentally controllable variables as

$$E_{fus} = 1.14\times10^5 B_e^{3.73} \varphi_p^{1.47} l_s^{1.5} r_c^{0.67}. \qquad (8)$$

The FRC poloidal flux and final FRC length are primarily a function of the scale of the formation sections positioned at each end of the device (see figures 2 and 3). To obtain the fusion gain, equation (8) must be normalized to the FRC energy acquired each pulse. The FRC energy can be stated as

$$E_{FRC} = \frac{3}{2} N k (T_e + T_i)\cdot \mathrm{Vol}_{FRC} \cong \frac{B_e^2}{2\mu_0} \pi r_s^2 l_s. \qquad (9)$$

Employing equation (7) again for the FRC radius, one has

$$G = \frac{E_{fus}}{E_{FRC}} = 0.093 B_e^{2.4} \varphi_p^{0.82} l_s^{0.5}. \qquad (10)$$

It is notable that the gain has no dependence on the compression coil radius, and only a fairly weak dependence on the FRC length. Gain contours as a function of the FRC poloidal flux and compression field are shown in figure 7.

This is not to say that one is free to pick any radius for the burn chamber compression coil. As was pointed out earlier,

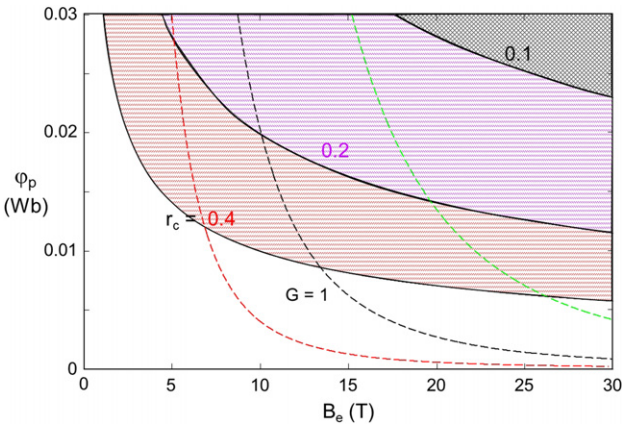

Figure 8. Gain plot as in figure 7 with regions of exclusion for different compression coil radii r_c, where an ion temperature was 9 keV and a FRC length $l_s = 1$ m were assumed.

there is the kinetic stability criterion, which was expressed as $S^*/\varepsilon < 5$. Stating this criterion in terms of the control variables

$$\frac{S^*}{\varepsilon} = \frac{2r_s}{l_s}\frac{r_s\omega_{pi}}{c} = 8.75 \times 10^3 \frac{B_e^{1/3}\varphi_p^{2/3}r_c^{2/3}}{l_s T_i^{1/2}} \leqslant 5, \qquad (11)$$

where the ion atomic number was assumed to be 2.5 for the D–T plasma. For kinetic and/or Hall effects to stabilize the FRC, the ion gyro-orbit must remain a significant fraction of the plasma radius (e.g. either a higher T_i or lower φ_p) with a reasonable assumption for the fusion ion temperature (9 keV), equation (11) expresses the stability limit on the amount of poloidal flux for a given coil radius and confining field:

$$\varphi_p \leqslant 0.0126 \frac{l_s^{3/2}}{B_e^{1/2} r_c}. \qquad (12)$$

The plot of the regions of the φ_p–B_e space of figure 7 that are excluded for various coil radii is shown in figure 8.

It is clear that to achieve fusion gain at the lowest possible compression field a coil radius of 0.2 m or less is desired, with a coil radius of less than 0.1 m ensuring kinetic stability for the largest range of both flux and compression field.

There are several reasons to keep the compression coil small. Certainly the amount of compression field energy required per pulse is thereby minimized, but perhaps more importantly, the wall loading per pulse is reduced as the ratio of wall surface area to reacting volume scales as $1/r_c$.

4. Pulsed FRC fusion reactor prototype

One is now in a position to determine the basic parameters of a fusion reactor based on the pulsed compression of the FRC. The initial design should aim to validate the concept with a device that is capable of attaining $G = 1$. The goal would be to demonstrate this with an experiment that would operate essentially in a single pulse mode ($R_p \gg 1$ Hz) to reduce the cost and complexity of the pulse power systems, but to do it in a manner that could evolve into a commercially viable device. This is deemed possible due to the several unique attributes of the concept that eliminate or significantly mitigate the major cost drivers inherent in the other approaches. For instance, with cyclical plasma generation the need for sustainment, fuelling and auxiliary heating systems, including current drive, is eliminated which could potentially simplify reactor operation. Having a transient burn, the vacuum boundary should be much easier to maintain thereby significantly reducing recycling, tritium retention and wall interaction issues. A conceptual design is illustrated in figure 9.

In figure 9 the radial scale has been exaggerated and the length of the burn region inside the compression coil has been foreshortened for purposes of illustration. The breeding blanket, which would immediately surround the high field chamber, is also not shown for clarity. The cross section of the burn region and blanket is illustrated in figure 10. There are several alternative possibilities for the configuration of compression coil and fusion blanket. The use of a beryllium inner wall as part of a flux concentrator and neutron multiplier is one possibility as indicated in the figure. Other arrangements include the use of a conventional multi-turn solenoid at the inner boundary. While the neutron fluence would no doubt limit the lifetime of such a coil, the linear, simply connected nature of the confinement system could make periodic replacement an acceptable arrangement. A structural analysis of these various options has yet to be carried out and would need to be performed to determine the best method for field creation in the burn chamber.

In order to make sure that the assumptions made in the prototype design are consistent with the scaling process of the FRC formation and merging demonstrated with the IPA results, several runs of the 2D MHD Moqui code were conducted using typical fields, voltages and fill inventories used in past FRC experiments for the FRC formation. The radial scale of the formation coils was set the same as the LSX FRC experiment [21]. The coil fields and timings were adjusted to produce the same supersonic FRCs as achieved in the IPA experiments with merging occurring in a compression coil with the same radius ($r_c = 0.1$). The major difference being that the compression field for the calculations was increased to 10 T. The results are displayed in figures 11 and 12.

The unique ability of the FRC plasmoid to be simultaneously translated and compressed over distances of several metres allows for the FRC formation and kinetic energy input to be added incrementally outside of the burn chamber and breeding blanket. This is clear from the time history of the ion temperature shown in figure 12. The ion temperature increases from a combination of pre-compression and kinetic conversion prior to the merging and final conversion in the compression chamber at 24 μs. In the process the ions receive the bulk of the heating. After the FRC merges and heats, any residual axial motion is only weakly damped as the FRC velocity is subsonic. There was sufficient reconnection in this calculation that the FRCs do not become separated even though the residual velocity is not small.

The compression of the FRC to high energy density can be performed inside a simple, small cylindrical coil set that is constructed for pulsed, high magnetic compression fields. This kind of magneto-kinetic heating is efficient and avoids the numerous challenges confronting steady-state approaches where large ports and sophisticated neutral beam devices are needed to create, heat, and possibly sustain the plasma currents.

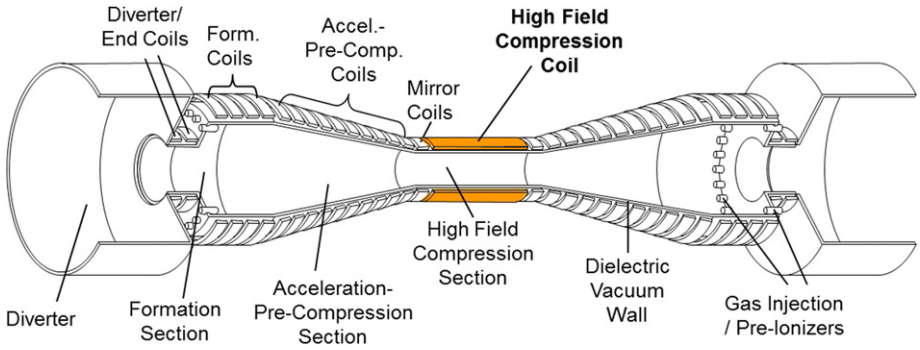

Figure 9. Conceptual depiction of a prototype fusion reactor based on the pulsed compression of the FRC.

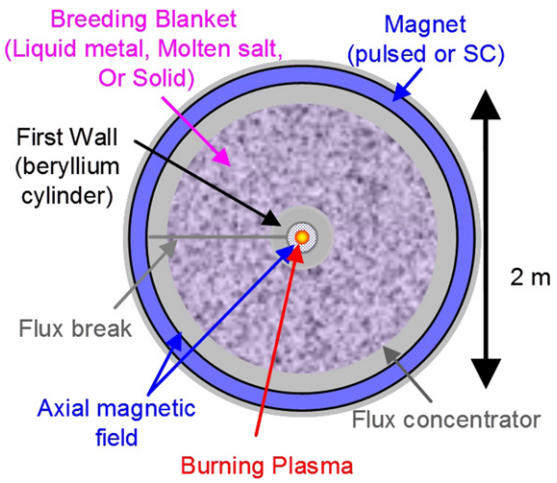

Figure 10. Midplane cross section of compression section with fissile–fussile breeding blanket.

These ancillary devices must also be co-located with the fusion reactor blanket and power processing systems making for a more complex and inefficient reactor.

Operation with tritium will necessitate recovery of unused fuel. A large divertor region is thus located at each end of the formation sections (see figure 9). The plasma exhaust (divertor) regions can be as large as desired and well removed from the reactor, eliminating critical power loading issues. As can be seen in figure 11, the entire high field reactor vacuum flux is external to FRC plasmoid flux and is thus essentially divertor flux. In a transient burn, the particle loss from the FRC will be overwhelmingly directed to the divertor regions as the axial flow time is many orders of magnitude smaller than the perpendicular particle diffusion time across the open flux region. The strong axial gradient magnetic field outside the burn chamber ensures that the plasma lost from the FRC remains contained in the divertor regions essentially eliminating tritium co-deposition and making the tasks of full tritium recovery and divertor maintenance much easier to carry out.

5. Discussion and conclusion

With the successful merging of supersonic FRCs in the IPA experiments, a method with the potential for the production of fusion energy in a simple and technologically appealing manner has been demonstrated. FRC plasmoids were brought to high temperature and density via a linear, sequenced array of low field compression coils establishing a means for obtaining fusion conditions remote from the plasma formation system. To obtain the requisite Lawson product a larger FRC must be formed, accelerated and compressed to higher fields. From the results of the IPA experiments together with equation (10), breakeven conditions will require an increase in poloidal flux which can be achieved by a radial scale increase of roughly a factor of three to a formation size similar to the LSX experiment [21]. The merging chamber would remain at 0.1 m radius but at much higher field (10 T). The same magneto-kinetic compression scheme as used on IPA would be extended in order to impel the FRC into the higher fields of the burn chamber.

The suitability of this approach to fusion or fusion–fission hybrid applications [22] is the consequence of the numerous critical advantages that significantly reduce the technological challenges, as well as the cost of development and operation. The more significant begin with the ability of the FRC plasmoid to be translated and merged where the FRC formation and kinetic energy input are added outside the burn chamber and realized only within the burn chamber as demonstrated in the IPA experiments. The plasma divertor region is well removed from the reactor, and can be scaled to eliminate any power loading issues. With the divertor located remotely in an essentially neutron-free environment, tasks such as full tritium recovery and divertor maintenance are made much easier to perform.

In order to rapidly spawn additional fusion systems, maintaining a low tritium inventory and creating more tritium than consumed will be essential. Due to the pulsed FRC reactor's linear, cylindrical geometry and the small scale of the fusion plasma compared with the neutron absorption region, the breeding blanket coverage can be optimized. It is critical that a sufficient number of energetic neutrons interact with lithium in the blanket to breed new tritium fuel. A high conversion efficiency of the fast fusion neutrons in the blanket surrounding the device makes significantly more fusion neutrons available for both fussile and fissile fuel generation as well as waste burning applications. The simply connected, linear geometry of the reactor vessel is also amenable to rapid and frequent first wall replacement if necessary. A fluid metal wall interface in this geometry is also feasible [23]. This would allow for operation at the highest power density, and resolve several plasma–material wall issues.

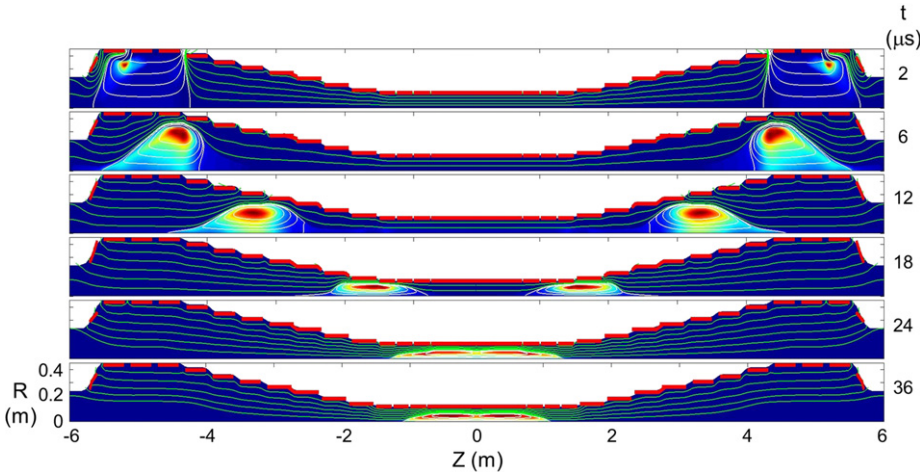

Figure 11. Field line and pressure contours from 2D MHD calculation of the formation merging and compression of the FRC in the prototype.

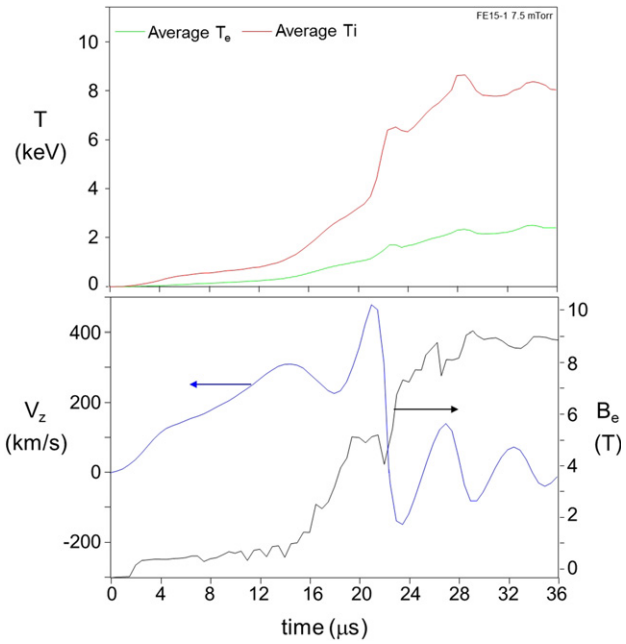

Figure 12. Top: the time history of the average electron and ion temperature inside the FRC. Bottom: the time history of the FRC axial velocity and external magnetic field at the midplane of the FRC.

There are also several critical attributes related to the unique nature of the FRC as a fusion plasma. Reactor costs will generally scale inversely with the fusion power density which in turn scales as $\beta^2 B^4$. The FRC has the highest β of all magnetically confined fusion plasmas, and the simple cylindrical nature of the confining field coils provides for the highest magnetic fields. Utilizing the FRC plasmoid for magnetic fusion energy thus represents the highest fusion power density that can be attained in a non-destructive, repetitive manner. As indicated in figure 10, the small ratio of the FRC volume to the neutron absorbing blanket volume provides for the maximum fusion power density obtainable without exceeding thermal limitations in the blanket. For hybrid operation, the small footprint allows for easy integration into existing fission power plant infrastructure. The reduced reactor scale also means much faster and far less expensive iterations during the development phase which will be essential to the integration of improvements and new technologies.

At first thought, it would appear that a pulsed system would be inferior to a steady system, primarily due to the advantages of self-sustainment (i.e. ignition). There are several limitations imposed by a steady fusion burn, not the least being constrained to an inherently low power density. As is now being realized, the steady burn does not easily allow for maintenance of the plasma–wall interface. The ability to maintain the critical balance between alpha heating and plasma losses in an ignited reactor is an open question; as is tritium retention, fuelling, burn diagnostics, plasma current sustainment, profile control, as well as several other device specific issues such as disruptions. By virtue of the cyclic nature of the burn, virtually all these issues are eliminated or significantly mitigated. Both fusion reactor gain and divertor wall loading can be readily regulated by the compression strength and repetition rate R_p. All of the D–T fuel can be introduced during the initial formation of the FRC plasmoid, eliminating the need for refuelling.

The major challenge for pulsed systems is operation at the highest efficiency possible in order to minimize what would otherwise be a large recirculating power fraction. Using pulsed magnetic fields to form, accelerate and compress the FRC to fusion conditions is efficient with Ohmic losses in the drive circuits as the primary loss channel. Employing a pulsed magnetic field also affords a unique opportunity for direct energy recovery. It has been appreciated in the past that pulsed systems employing flux compression can realize direct recovery of the fusion alpha energy [24]. For the pulsed compression of the FRC this takes the form of the back emf experienced by the compression circuit due to the increase in FRC plasmoid pressure from the presence of the fusion alphas. This push-back during the natural oscillatory behaviour of the compression circuit causes the energy storage capacitors to be recharged to greater energy from the increased expansion energy of the FRC. A key technology for such a system is the use of an opening switch to allow this energy to then be stored for the next pulse. This appears feasible as the voltages

and energies envisioned for the prototype are within the range of what can be achieved with current solid state switches and power delivery systems [25]. Additional recuperative operation of all the magnetic field circuits would provide for a way to significantly reduce the energy losses to primarily that of the FRC itself. Even that energy may be recoverable in some measure by direct conversion in the divertor as the plasma energy loss is primarily in the form of a high energy, directed plasma jet at the divertor entrance [23, 26]. The capability to make use of the plasma, fusion and electrical energy in an efficient manner is unique to the concept described here, and is critical for the commercial application of fusion to be realized without resorting to a larger scale, higher fusion gain system.

Possibly the most underappreciated advantage of a pulsed system comes from the ability to evaluate key performance milestones with single pulses. This minimizes neutron activation during development and further reduces cost as much simper and less robust pulse power systems can be employed. Given the scaling and the desire to optimize at smaller radius and higher power density, it is worth determining the parameters of a device capable of a gain of five. From equation (10) the following values will yield such a gain:

$$l_s = 2\,\mathrm{m} \quad \varphi_p = 25\,\mathrm{mWb} \qquad B_e = 16\,\mathrm{T} \Rightarrow Q = 5. \qquad (13)$$

With a compression coil radius $r_c = 0.2\,\mathrm{m}$, the FRC should remain well below the kinetic stability limit given in equation (12) even prior to full compression. The fusion energy per pulse is given by equation (8) and for the assumed parameters yields $E_{fus} = 14\,\mathrm{MJ}$. The repetition rate R_p is determined by the wall loading limits. Taking advantage of the translatability of the burning FRC, the compression section can be made much longer than the FRC so that the drifting FRC deposits the fusion energy along a series of compression coil sections. Alternatively, the FRCs can be merged and brought to rest in a different part of the elongated compression chamber with each pulse. In either case, the repetition rate will likely never exceed 2–4 Hz for average power of 40 to 60 MW in order to maintain the average neutron fluence below $4\,\mathrm{MW\,m^{-2}}$. The low frequency minimizes the pulse power issues as well as any pump out concerns.

A low total fusion yield would at first seem restrictive. It does, however, have several advantages. With eventual fusion plant power output in the 200 to 500 MW range, the pulsed FRC reactor can be modularized. The investment-intensive energy input and fuel recovery systems can be used to power multiple, relatively inexpensive, easily replaceable burn chambers. This will be particularly important in the early stages of deployment when reliability and maintenance schedules will be less well understood.

In summary, with the repetitive and efficient generation of FRC plasmoids, brought to high temperature and density as they are injected into the burn chamber, a compact, low-cost fusion neutron source can be achieved. At a minimum it would be an attractive source for fast neutron-based applications such as isotope production, fissile fuel breeding and fission waste transmutation. The expectation is that with the successful demonstration of a prototype scale device, a viable alternative for fusion energy production can be rapidly developed at an affordable cost, and will spur a renewed urgency to perform the required reactor development on a timescale that will allow fusion to be a major player in the world's energy future.

Acknowledgments

The authors would like to thank Dr David Kirtley for his assistance in calibrating the neutron detector response, and Dr Samuel Andreason for invaluable contributions to the design and construction of several electronic components. The work was partially supported by grants from the US Department of Energy.

References

[1] Tuszewski M. 1988 *Nucl. Fusion* **28** 2033
[2] Tuszewski M., Barnes D.C., Rej D.J. and Taggart D.P. 1991 *Phys. Fluids* B **3** 2205
[3] Armstrong W.T. *et al* 1981 *Phys. Fluids* **24** 2068
[4] Slough J.T. *et al* 1995 *Phys. Plasmas* **2** 2286
[5] Slough J. *et al* 2006 *J. Fusion Energy* **26** 199
[6] Votroubek G., Slough J., Andreason S. and Pihl C. 2008 *J. Fusion Energy* **27** 123
[7] Slough J. and Milroy R. 2010 *J. Fusion Energy* **29** 567
[8] Tahara H., Kagaya Y. and Yoshikawa T. 1997 *J. Propul. Power* **13** 651
[9] Guo H.Y., Hoffman A.L., Miller K.E. and Steinhauer L.C. 2004 *Phys. Rev. Lett.* **92** 245001
[10] Binderbauer M.W. *et al* 2010 *Phys. Rev. Lett.* **105** 045003
[11] Ono Y., Yamada M., Akao T., Tajima T. and Matsumoto R. 1996 *Phys. Rev. Lett.* **76** 3328
[12] Milroy R.D. and Brackbill J.U. 1982 *Phys. Fluids* **25** 775
[13] Yamada M. *et al* 1990 *Phys. Rev. Lett.* **65** 721
[14] Birn J. *et al* 2005 *Geophys. Res. Lett.* **32** L06105
[15] Sovinec C.R. *et al* 2004 *J. Comput. Phys.* **195** 355
[16] Milroy R.D., Macnab A.I.D., Kim C.C. and Sovinec C.R. 2008 *J. Fusion Energy* **27** 73
[17] Rej D.J. *et al* 1992 *Phys. Fluids* B **4** 1909
[18] Milroy R.D. and Steinhauer L.C. 2008 *Phys. Plasmas* **15** 022508
[19] Hoffman A.L. and Slough J.T. 1993 *Nucl. Fusion* **33** 23
[20] Chrien R.E. and Okada S. 1987 *Phys. Fluids* **30** 3574
[21] Slough J.T. *et al* 1992 *Phys. Rev. Lett.* **69** 2212
[22] Slough J., Kirtley D., Pihl C., Votroubek G. and Wallace P. 2010 The pulsed high-density frc as a neutron source for fusion–fission hybrid applications p 70 http://www.science.doe.gov/ofes/FF_Hybrid_Report_Final.pdf
[23] Harms A.A., Schoepf K.F., Miley G.H., Kingdom D.R. 2002 *Principles of Fusion Energy* (Singapore: World Scientific) pp 267–77
[24] Moir R.W. 1997 *Nucl. Fusion* **37** 557
[25] Pokryvailo A., Carp C. and Scapellati C. 2010 *IEEE Trans. Plasma Phys.* **38** 2734
[26] Kulcinski G.L. *et al* 1991 *Fusion Technol.* **19** 791